Sarah Patumona Manalu, Thillai Sivakumar Natarajan, Manuel De Guzman, Ya-Fen Wang, Tien-Chin Chang, Feng-Chi Yen and Sheng-Jie You*

Synthesis of ternary g-C_3N_4/Bi_2MoO_6/TiO_2 nanotube composite photocatalysts for the decolorization of dyes under visible light and direct sunlight irradiation

https://doi.org/10.1515/gps-2017-0077
Received May 26, 2017; accepted October 6, 2017; previously published online January 18, 2018

Abstract: Novel ternary nanocomposite photocatalysts based on g-C_3N_4/Bi_2MoO_6/TiO_2 nanotube were synthesized using simple solid combustion, hydrothermal and wetness impregnation methods. The structural and morphological properties of the synthesized photocatalysts were systematically characterized using powder X-ray diffraction (XRD), Fourier transform infrared spectroscopy and scanning electron microscopy (SEM). The crystal structure and phase purity of unitary, binary, and ternary photocatalysts were confirmed by XRD analysis. The SEM analysis reveals the tubular morphology of the TiO_2 nanotube, and the presence of Ti, C, N, Bi, Mo, O, C, and N in the ternary composites was confirmed by EDX analysis. The photocatalytic decolorization efficiency of the ternary composites was evaluated by monitoring the decolorization of reactive black 5 and methylene blue dyes under visible light and direct sunlight irradiation, and these ternary composites were compared with binary composites and unitary photocatalysts in terms of the decolorization efficiency. After five cycles of adsorption and decolorization reactions, it was confirmed that the ternary composite photocatalysts were highly stable and reusable. From the results, we conclude that ternary composites (g-C_3N_4/Bi_2MoO_6/TiO_2 nanotube) are efficient photocatalysts for the decolorization of dyes.

***Corresponding author: Sheng-Jie You,** Department of Environmental Engineering, Chung Yuan Christian University, Chungli 320, Taiwan, e-mail: sjyou@cycu.edu.tw
Sarah Patumona Manalu, Manuel De Guzman and Ya-Fen Wang: Department of Environmental Engineering, Chung Yuan Christian University, Chungli 320, Taiwan
Thillai Sivakumar Natarajan: Department of Environmental Engineering, Chung Yuan Christian University, Chungli 320, Taiwan; and School of Chemical and Bioprocess Engineering, Engineering and Materials Science Centre, University College Dublin (UCD), Belfield, Dublin 4, Ireland
Tien-Chin Chang: Institute of Environmental Engineering and Management, National Taipei University of Technology, Taipei 106, Taiwan
Feng-Chi Yen: Department of Environmental Engineering, Chung Yuan Christian University, Chungli 320, Taiwan; and Industrial Development Bureau, Ministry of Economic Affairs, Taipei 10651, Taiwan

Keywords: Bi_2MoO_6; dye decolorization; g-C_3N_4; sunlight irradiation; ternary composite; TiO_2 nanotube; visible light.

1 Introduction

Water pollution is a critical global problem; it poses a serious threat to our health. Dye pollutants are the principal constituents in industrial wastewater. Numerous studies about physical, biological, thermal, and chemical treatments for the removal of dyes from industrial wastewater have been investigated. However, these are energy intensive, transforming the pollutants from one phase to another, which creates secondary pollution and high operating cost over a long term, and are economically not viable [1–5]. To overcome these constraints, advanced oxidation processes (AOPs) are applied, as AOPs have been considered as one of the most promising techniques for degrading various pollutants. Among the AOPs, photocatalysis is a promising and environmentally benign technology for treating industrial wastewater in the presence of light irradiation using semiconductors as photocatalysts, which result in less residual waste [6–8]. The discovery by Fujishima and Honda on the photoelectrochemical splitting of water using a TiO_2 semiconductor [9] made a significant contribution toward the use of TiO_2 as a photocatalyst for the degradation of various pollutants. TiO_2 has been extensively used because of its photostability, availability, biological inertness, low energy consumption, high photocatalytic activity, environmental friendliness, and ability to prevent the formation of undesirable by-products [10–12]. However, the low visible light response of TiO_2 (high band gap, 3.2 eV) and its high recombination rate of photogenerated charge carriers decreases the photocatalytic activity. In addition, it possesses a low surface area, which leads to low adsorption of pollutants on a catalyst surface and decreases their activity.

The surface area of TiO_2 has been improved by synthesizing different morphologies of TiO_2. The synthesized TiO_2 nanotube has received significant attention because of its high specific surface area and pore volume, numerous

surface defects, and ion-exchangeable property. These offer a discrete environment for adsorption of large molecules such as dyes [13, 14]. However, the photocatalytic activity of the TiO_2 nanotube under visible light is poor because of its high band gap and the charge carrier recombination rate. Therefore, to make use of this high-surface area TiO_2 nanotube, it has been combined with different metals and non-metals and low band gap semiconductors; this would enhance the visible light response and charge carrier transfer rate [15–17]. Nevertheless, the stability of the TiO_2 nanotube loaded with metals and non-metals is poor; problems with recyclability and the reproducibility of the degradation results remain unresolved. Subsequently, the making of the composite TiO_2 nanotube with low-band gap semiconductors is highly attractive and improves its visible light response and the charge carrier transfer rate. Among the low-band gap semiconductors, photocatalysts based on graphitic carbon nitride (g-C_3N_4) and bismuth have become highly attractive because of their narrow band gap (–2.6 to 2.7 eV) and could be used for the absorption of higher concentrations of visible light and higher rates of charge carrier transfer [18–21]. Moreover, bismuth is a p-block metal with a d^{10} electronic configuration, which is beneficial for promoting the mobility of photogenerated carriers and used for the preparation of efficient visible light-responsive photocatalytic materials with high stability. Among these, Bi_2MoO_6 has received significant attention and demonstrated distinguished photocatalytic activities under visible light irradiation because of its suitable band gap (2.67 eV) and excellent intrinsic structures such as dielectric nature, catalytic behavior, and luminescence [22–24]. Similarly, g-C_3N_4 is a metal-free semiconductor, composed of only two earth-abundant elements (carbon and nitrogen); the position of the g-C_3N_4 conduction band (CB) is extremely negative (–1.135 vs. NHE); thus, its photogenerated electrons have a strong reducing ability [20, 25, 26]. Subsequently, these Bi_2MoO_6 and g-C_3N_4 were combined with the TiO_2 nanoparticles separately, which expanded the visible light response of TiO_2 and improved the photogenerated charge carrier separation and transfer rate. Sridharan et al. [27] synthesized composite photocatalysts (g-C_3N_4/TiO_2) that demonstrated fast electron transfer at the interface between g-C_3N_4 and TiO_2, which improved their visible light photocatalytic activity in the degradation of methylene blue dye and the reduction of Cr(VI) ions. Shen et al. [28] prepared mesoporous nanocomposites (g-C_3N_4/TiO_2) for the degradation of methyl orange dye. Jo and Natarajan [29] studied the influence of TiO_2 morphology on the photocatalytic decomposition efficiency of g-C_3N_4/TiO_2 composites by isoniazid degradation. Similarly, the loading of Bi_2MoO_6 on TiO_2 enhanced the visible response of TiO_2 and the charge carrier separation and transfer rate, which led to enriched photocatalytic activity. Li et al. [30] deposited the Bi_2MoO_6 nanoparticles on the TiO_2 nanorod through a solvothermal method for the degradation of methylene blue dye under visible light irradiation. Zhang et al. [31] synthesized composite nanofibers (Bi_2MoO_6/TiO_2) using an electrospinning method for the degradation of rhodamine B dye. Similarly, different studies have been reported on the synthesis of composite photocatalysts (g-C_3N_4/TiO_2 and Bi_2MoO_6/TiO_2 nanoparticle) for the degradation of pollutants [32–36]. Recently, the visible light response of TiO_2 and charge carrier separation and transfer rate have been improved further by synthesizing ternary composite photocatalysts [37]. However, the literature on the synthesis of binary and ternary composites based on the TiO_2 nanotube, Bi_2MoO_6, and g-C_3N_4 is scarce. Moreover, the visible light photocatalytic efficiency of the aforementioned composites was investigated mainly in the presence of artificial visible light; therefore, the activity evaluation under direct sunlight is seldom reported.

In this study, we report the synthesis of ternary composite photocatalysts comprising the TiO_2 nanotube loaded with Bi_2MoO_6 and g-C_3N_4 through simple solid combustion, hydrothermal and wetness impregnation methods. Subsequently, the photocatalytic efficiencies of the synthesized photocatalysts were investigated through the decolorization of reactive black 5 and methylene blue dyes under visible light and direct sunlight irradiation. The ternary composites demonstrate a higher photocatalytic activity in decolorizing dyes when compared with unitary and binary composite photocatalysts under the same reaction conditions.

2 Materials and methods

Commercial reagents were provided and used without further purification. Bismuth(III) nitrate pentahydrate ($Bi(NO_3)_3 \cdot 5H_2O$), sodium molybdate dihydrate ($Na_2MoO_4 \cdot 2H_2O$), and hydrochloric acid (HCl) were purchased from Sigma Aldrich (Saint Louis, MO, USA). Urea was procured from Bio Basic Inc. (Markham, ON, Canada). Commercial TiO_2 P25 was purchased from Uni Region Biotech, USA. Methanol was purchased from M. Tedia Inc. (Fairfield, OH, USA). Sodium hydroxide (NaOH) was purchased from Nihon Shiyaku Reagent (Tokyo, Japan). Potassium bromide was procured from Fluka Analytical (Saint Louis, MO, USA). Reactive black 5 and methylene blue dyes were purchased from Merck Millipore (Darmstadt, Germany).

2.1 Synthesis of Bi_2MoO_6 nanoplate photocatalyst

Bi_2MoO_6 nanoplates were synthesized using a hydrothermal method [38]. A mixture of $Bi(NO_3)_3 \cdot 5H_2O$ and $Na_2MoO_4 \cdot 2H_2O$ was dissolved in deionized water, and then, the pH was adjusted to 6.0 by adding HCl. After that, it was stirred for 1 h at room temperature. The mixture was transferred to a Teflon-lined stainless steel autoclave and heated

at 453 K for 20 h in an electric oven. After 24 h, the autoclave was cooled to room temperature. The obtained yellowish precipitate was centrifuged, washed with distilled water, and dried at 353 K for 24 h.

2.2 Synthesis of g-C_3N_4 photocatalyst

g-C_3N_4 was prepared through the direct calcination of urea [39]. Urea was placed in a crucible, which was covered with a lid and heated at 773 K for 3.5 h. Subsequently, the crucible was cooled to room temperature, and the obtained yellow g-C_3N_4 product was collected and stored for further composite synthesis.

2.3 Synthesis of TiO_2 nanotube photocatalyst

The TiO_2 nanotube was synthesized using TiO_2 P25 nanoparticles through a hydrothermal method [40]. First, a commercial TiO_2 P25 was added to a 10-N NaOH solution, and it was stirred vigorously at room temperature and transferred to a Teflon-lined stainless steel autoclave and heated at 403 K for 48 h. Afterward, the autoclave was allowed to cool to room temperature, and the obtained nanotube was centrifuged and washed with distilled water until the pH of the filtrate was approximately 6–7. Then, the nanotube was treated with 0.1 M HCl solution, which was later stirred overnight at room temperature. Thereafter, the nanotube was centrifuged, washed with distilled water, and dried in an oven at 343 K for 12 h. The dried nanotube was calcined in a tubular furnace at 523 K for 2 h and used for further composite synthesis.

2.4 Synthesis of binary (g-C_3N_4/Bi_2MoO_6) and ternary (g-C_3N_4/Bi_2MoO_6/TiO_2 nanotube) composite photocatalysts

g-C_3N_4/Bi_2MoO_6 and g-C_3N_4/Bi_2MoO_6/TiO_2 nanotube composites were synthesized using a wet impregnation method. Binary composites (g-C_3N_4/Bi_2MoO_6) with different weight percentages of g-C_3N_4 were synthesized. Initially, an appropriate amount of Bi_2MoO_6 was dispersed in 100 ml of methanol under sonication. After that, the required amount of g-C_3N_4 was added and stirred for 24 h at ambient temperature. After the complete evaporation of methanol, the obtained g-C_3N_4/Bi_2MoO_6 composites were dried at 353 K for 12 h and, then, calcined at 573 K for 1 h. The prepared binary composites (g-C_3N_4/Bi_2MoO_6) with different weight percentages of g-C_3N_4 were abbreviated as x%g-C_3N_4/Bi_2MoO_6(x = 5%, 10%, 30%, 50% and 70%). In the preparation of ternary nanocomposites (g-C_3N_4/Bi_2MoO_6/TiO_2 nanotube), different amounts of TiO_2 nanotubes were added to the binary composites, and the same aforementioned procedure was followed.

2.5 Characterization

X-ray diffraction (XRD) analysis was performed using a Bruker D8 Advance Eco diffractometer (Bruker Corporation, San Jose, CA, USA) to identify the crystal structure of the photocatalysts. The purity of the synthesized photocatalysts and their elemental constituents were determined using energy-dispersive X-ray (EDX) spectroscopy (Hitachi Co., Tokyo, Japan). The morphologies of the photocatalysts were examined using a Hitachi S-4800 scanning electron microscope (SEM) (Hitachi Co., Tokyo, Japan). The Fourier transform infrared (FT-IR) spectra of the samples were recorded using a Jasco FT-IR-6500 Fourier transform infrared spectrometer (JASCO International Co. Ltd., Tokyo, Japan) over the wavenumber range 400–4000 cm^{-1} (KBr pellets were used).

2.6 Photocatalytic activity

The photocatalytic activity of the synthesized unitary, binary, and ternary composites was evaluated by studying the decolorization behavior of an aqueous dye solution in the presence of visible light

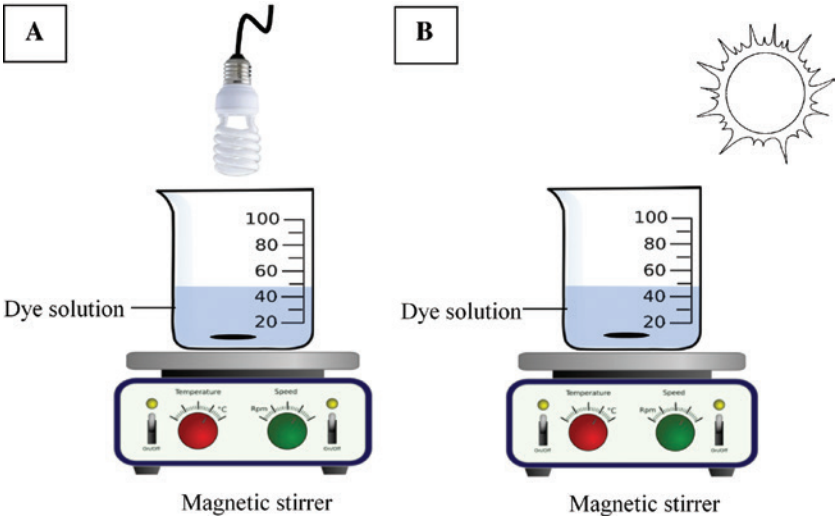

Figure 1: Experimental setup for the photocatalytic decolorization of dyes using synthesized photocatalysts under (A) visible light and (B) direct sunlight irradiation.

(Figure 1A) and direct sunlight irradiation (Figure 1B). Reactive black 5 and methylene blue dyes were chosen as target pollutants for decolorization studies. In the decolorization experiment, 0.5 g/l of photocatalyst and 100 ml of dye solution (10 mg/l) were placed in a beaker, and the photocatalyst was dispersed under sonication for 2 min. Prior to light irradiation, the reaction mixture was stirred under dark atmospheric conditions to obtain an adsorption-desorption equilibrium between the photocatalyst and the dye solution. Afterward, the reaction mixture was exposed to light irradiation, and the dye solution was withdrawn at predetermined time intervals for absorbance measurements by using a UV-vis spectrophotometer (Genesys 10s UV-Vis spectrophotometer). Before the UV analysis, the catalyst particles were separated through centrifugation; then, the absorbance for reactive black 5 and methylene blue dyes was measured at λ_{max} = 595 nm and λ_{max} = 665 nm, respectively. The concentration of the decolored dye solutions was determined using their calibration curves, and the percentage decolorization was calculated.

3 Results and discussion

3.1 X-ray diffraction and Fourier transform infrared analyses

The phase purity and crystallinity of the synthesized composites were determined using XRD, and the results are shown in Figure 2. Figure 2A presents the XRD patterns of the following: (1) synthesized g-C_3N_4, Bi_2MoO_6, and TiO_2 nanotube photocatalysts; (2) inorganic crystal structure database (ICSD) for Bi_2MoO_6 and TiO_2 nanotube; and (3) commercial TiO_2 P25. The synthesized g-C_3N_4 reveals two distinct diffraction peaks at 13.04° and 27.40°, which correspond to (100) and (002) diffraction planes of the graphite-like structure of g-C_3N_4, respectively. Moreover, the peak at 13.04° is attributed to the (100) plane of the tri-s-triazine unit of g-C_3N_4; the peak at 27.40° corresponds to the characteristic inter-planar stacking of the conjugated aromatic systems and the interlayer structural packing of the (002) plane of graphite-like materials [29]. For Bi_2MoO_6, strong diffraction peaks at 2θ = 11.00°, 28.55°, 32.66°, 33.24°, 36.17°, 47.42°, 55.61°, 56.43° and 58.54° can be assigned to (0 2 0), (1 3 1), (2 0 0), (2 1 0), (1 5 1), (2 6 0), (3 3 1), (1 9 1) and (2 6 2) crystal planes, respectively. For the TiO_2 nanotube, the diffraction peaks at 2θ = 25.4°, 39°, 48.05°, 55° and 63° are indexed to the (1 0 1), (1 1 2), (2 0 0), (2 1 1) and (2 0 4) planes of the anatase phase of TiO_2, respectively. The XRD patterns of the synthesized Bi_2MoO_6 and TiO_2 nanotube match their corresponding ICSD data well. Furthermore, no peaks correspond to layered titanates, and a change in the anatase phase was observed after the hydrothermal treatment of TiO_2 nanocrystalline powder. Therefore, the XRD pattern validates the complete transformation of TiO_2 nanoparticles to nanotube, and the TiO_2 nanotube comprised the anatase phase only [40]. Figure 2B presents the XRD patterns of the following photocatalysts: (1) g-C_3N_4/Bi_2MoO_6/TiO_2 nanotube, (2) Bi_2MoO_6/TiO_2 nanotube, (3) g-C_3N_4/Bi_2MoO_6 and (4) g-C_3N_4/TiO_2 nanotube. Peaks corresponding to g-C_3N_4 in binary (g-C_3N_4/Bi_2MoO_6) and ternary (g-C_3N_4/Bi_2MoO_6/TiO_2 nanotube) composites were not observed. This may be due to the diffraction peak of g-C_3N_4 at 27.40° being superimposed with the Bi_2MoO_6 diffraction peak at 28.55°.

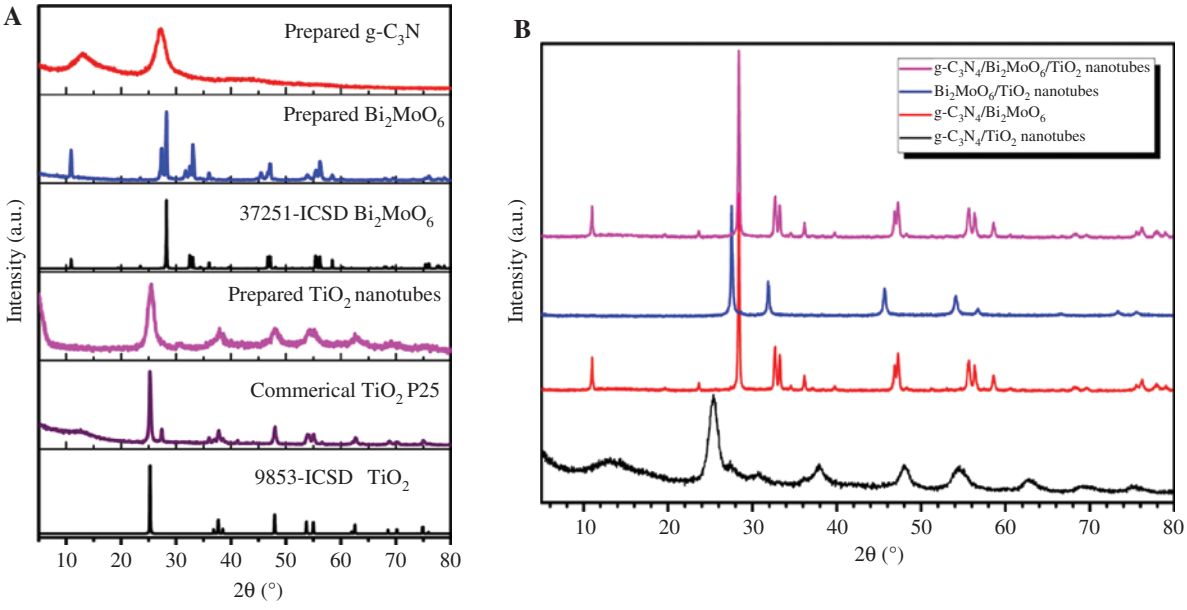

Figure 2: XRD patterns of (A) g-C_3N_4, Bi_2MoO_6, and TiO_2 nanotube and (B) binary and ternary composite photocatalysts.

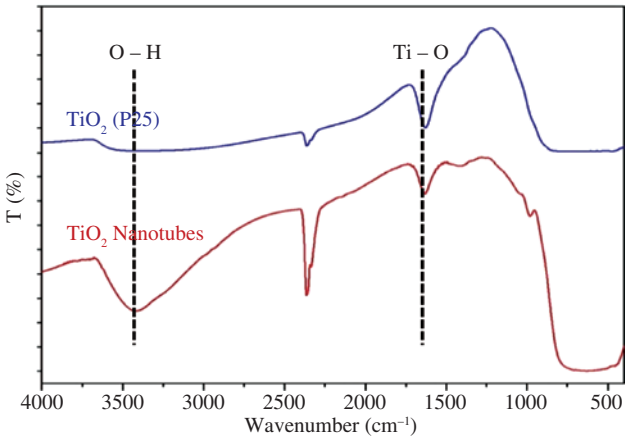

Figure 3: FT-IR spectra of TiO_2 P25 and TiO_2 nanotube photocatalysts.

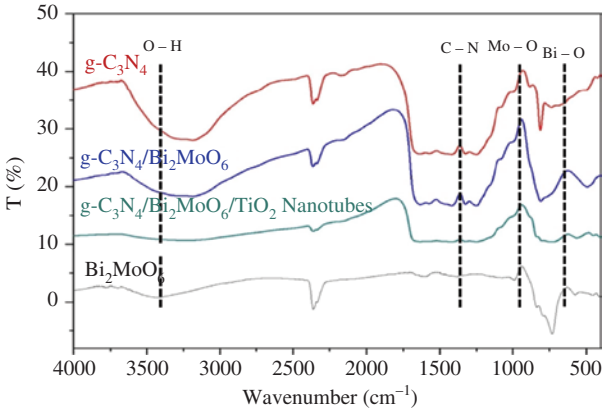

Figure 4: FT-IR spectra of g-C_3N_4, Bi_2MoO_6, g-C_3N_4/Bi_2MoO_6, and g-C_3N_4/Bi_2MoO_6/TiO_2 nanotube photocatalysts.

Similarly, the TiO_2 nanotube peak was not observed in the ternary composite because of the low concentration of TiO_2 nanotube in the composite. However, the g-C_3N_4 presence was clearly observed at $2\theta = 13°$ and 27° in the g-C_3N_4/TiO_2 nanotube composite. From the XRD patterns, we conclude that unitary, binary, and ternary composite photocatalysts were successfully synthesized, and the introduction of g-C_3N_4 and TiO_2 nanotube did not change the crystal structure of Bi_2MoO_6 in the ternary composite.

Figure 3 shows the FT-IR spectra of TiO_2 P25 and the TiO_2 nanotube. The bands at 3420 and 1629 cm^{-1} in the TiO_2 nanotube are attributed to the stretching and bending vibrations of the water molecule hydroxyl groups present on the surface of the TiO_2 nanotube. The higher intensity of the hydroxyl group peaks in the TiO_2 nanotube, relative to that in TiO_2 P25, and indicates that the surface of the TiO_2 nanotube contains a higher concentration of hydroxyl groups. This enhancement in the surface hydroxyl groups favors the adsorption capability of the TiO_2 nanotube and enhances its photocatalytic decolorization efficiency. Figure 4 displays the FT-IR spectra of g-C_3N_4, g-C_3N_4/Bi_2MoO_6, g-C_3N_4/Bi_2MoO_6/TiO_2 nanotube and Bi_2MoO_6. In the spectrum of g-C_3N_4, the strong peaks at 3420 and 3200 cm^{-1} can be ascribed to the absorbed water molecules and stretching mode of N–H, respectively. Four peaks at 1250, 1325, 1420 and 1572 cm^{-1} observed in g-C_3N_4 are related to the typical stretching modes of the CN heterocycle. For Bi_2MoO_6, the peaks at 400–900 cm^{-1} originate from Bi–O, Mo–O stretching and Mo–O–Mo bridging stretching modes. The distinct absorption peaks of g-C_3N_4 and Bi_2MoO_6 were also observed in the composites of g-C_3N_4/Bi_2MoO_6 and g-C_3N_4/Bi_2MoO_6/TiO_2 nanotube.

3.2 Morphology

The morphological properties of the synthesized photocatalysts were characterized using SEM at different magnifications, and the results are shown in Figure 5. The SEM image of the Bi_2MoO_6 photocatalyst (Figure 5A) shows a plate-like structure in which the length was in the range of nanometer scale. The SEM image of g-C_3N_4 (Figure 5B) illustrates that it exhibits a thin sheet-like structure with wrinkled surface and irregular shapes. Figure 5C describes that the commercial TiO_2 P25 particles were spherical in shape. The SEM image of the synthesizedTiO_2 nanotube (Figure 5D) indicates that several long fibers were assembled together, with the diameter in the range of 10–30 nm. A binary composite photocatalyst (g-C_3N_4/Bi_2MoO_6) reveals a structure comprising two layers of g-C_3N_4 nanosheets and Bi_2MoO_6 nanoplates (Figure5E). For the ternary composite photocatalyst (g-C_3N_4/Bi_2MoO_6/TiO_2 nanotube), a three-layered structure is indicated in Figure 5F. The intimate contact between these semiconductors could enhance the charge carrier separation and transfer rate and photocatalytic decolorization efficiency.

3.3 Energy-dispersive X-ray spectroscopic analysis

The presence of Bi_2MoO_6 and g-C_3N_4 in the ternary composite was confirmed by EDX analysis. Figure 6 illustrates the EDX spectrum of a ternary composite photocatalyst (g-C_3N_4/Bi_2MoO_6/TiO_2 nanotube). It indicates only the presence of Bi, Mo, O, C, N and Ti peaks in the composite, without the presence of any other characteristic peaks. This result confirms the successful synthesis of the ternary g-C_3N_4/Bi_2MoO_6/TiO_2 nanotube photocatalyst; it contains

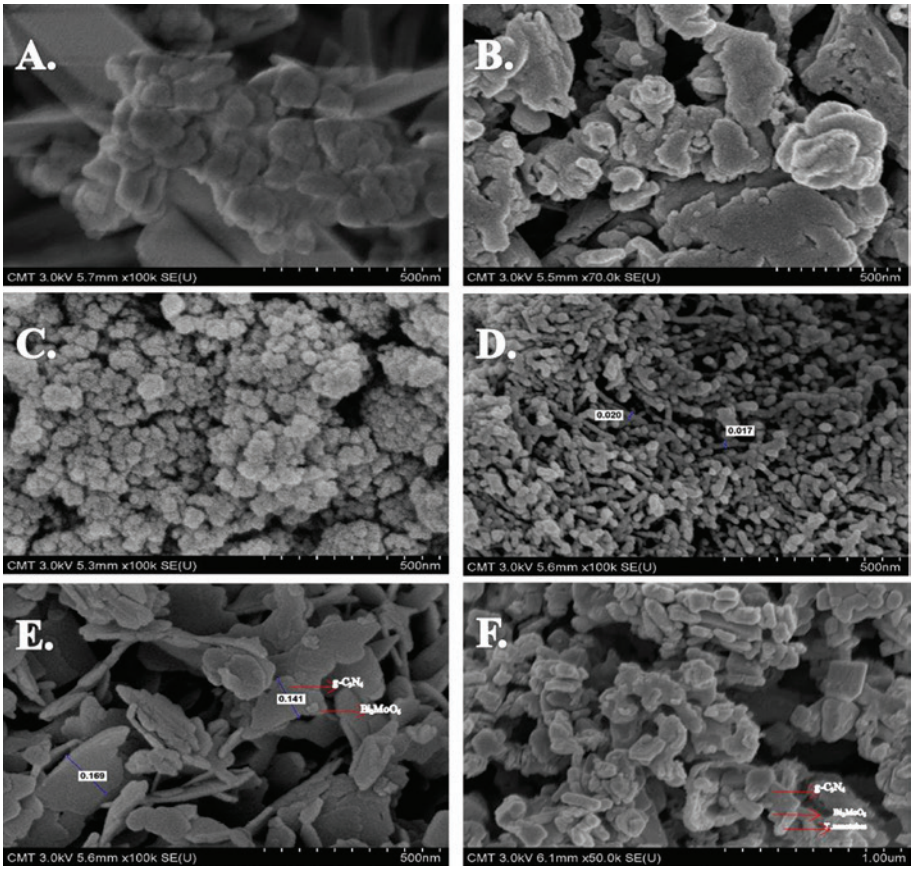

Figure 5: SEM images of (A) Bi_2MoO_6, (B) g-C_3N_4, (C) TiO_2 P25, (D) TiO_2 nanotube, (E) g-C_3N_4/Bi_2MoO_6, and (F) g-C_3N_4/Bi_2MoO_6/TiO_2 nanotube photocatalysts.

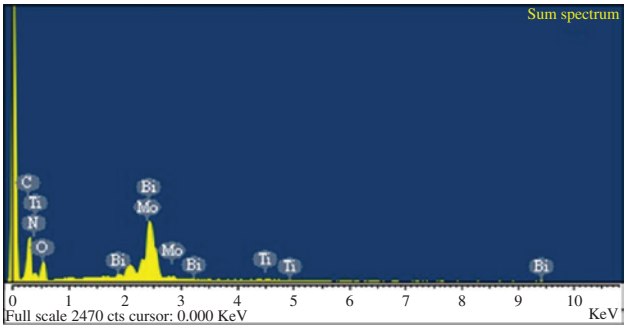

Figure 6: EDX spectra of a ternary composite photocatalyst (g-C_3N_4/Bi_2MoO_6/TiO_2 nanotube).

no impurities, which supports the powder XRD and FT-IR results.

3.4 Photocatalytic performance

Initially, the photocatalytic performance of unitary photocatalysts (g-C_3N_4, TiO_2 nanotube, Bi_2MoO_6, and P25 TiO_2) was investigated by decolorizing reactive black 5 with 0.5 g/l of catalyst under visible light irradiation, and the results are shown in Figure 7A. The results reveal that no decolorization was observed under blank conditions (without a catalyst). For Bi_2MoO_6 and P25 TiO_2, 18.9% and 51.68% of reactive black 5 was decolorized after 5 h of reaction. For g-C_3N_4 and the TiO_2 nanotube, the percentage decolorization of reactive black 5 was enhanced to 88.31% and 96.14%, respectively. This significant enhancement in the photocatalytic activity is due to the layered and tubular structure of g-C_3N_4 and TiO_2, which enhances the adsorption quantity of reactive black 5 on these photocatalysts. Among the photocatalysts, the TiO_2 nanotube exhibited the highest adsorption ability for reactive black 5, which leads to enriched photocatalytic decolorization efficiency.

The photoactivity of the binary photocatalyst (g-C_3N_4/Bi_2MoO_6) with different amounts of g-C_3N_4 (5–70%) was evaluated in terms of the decolorization of reactive black 5, and the results are shown in Figure 7B. The results reveal that the percentage decolorization of reactive black 5 increased from 18.9% (Bi_2MoO_6) to 27.54%, 91.20% and 94.09% for 5%, 10% and 30% loading of

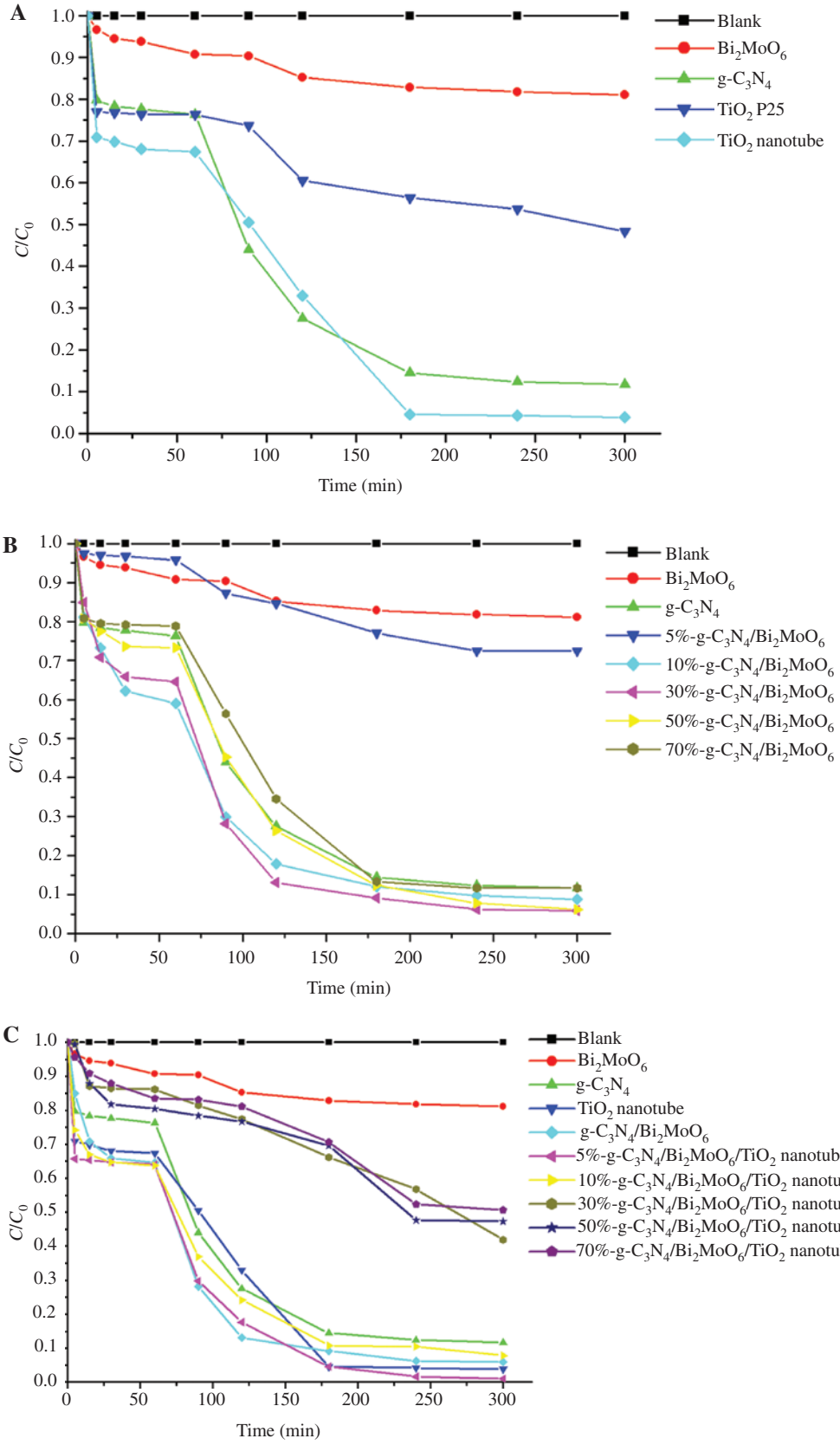

Figure 7: Photocatalytic decolorization of reactive black 5 caused by (A) unitary, (B) binary composite, and (C) ternary composite photocatalysts under visible light irradiation.

g-C_3N_4, respectively; increasing further the g-C_3N_4 loading to 50% and 70% decreased the percentage decolorization of reactive black 5 to 93.81% and 88.27%, respectively. The decreased photocatalytic decolorization efficiency at higher g-C_3N_4 loadings was due to the shielding effect of the added g-C_3N_4, which led to a decrease in the light intensity reaching the catalyst surface and a lowering of the generation of photogenerated charge carriers. Therefore, 30% g-C_3N_4 loading is the optimum amount, which was used for further ternary composite synthesis. The photocatalytic activity of the ternary composite with different loadings of the TiO_2 nanotube (5–70%) was determined, and the results are shown in Figure 7C. The results demonstrate that the ternary composite (5% TiO_2 nanotube loaded with 30% g-C_3N_4/Bi_2MoO_6) exhibits a higher percentage decolorization (99.02%) of reactive black 5; increasing further the TiO_2 nanotube loading to 10%, 30%, 50% and 70% resulted in a decrease in the dye percentage decolorization. From the results, it is observed that 30% g-C_3N_4/Bi_2MoO_6/5%TiO_2 nanotube is the optimum catalyst for the highest percentage decolorization of reactive black 5. We evaluated the photocatalytic decolorization efficiency of this optimum catalyst on the cationic methylene blue; the results reveal that 73.61% of methylene blue was decolorized.

In addition to the aforementioned initial decolorization studies, we also studied the effect of different parameters, such as the catalyst amount, initial dye concentration, pH, and temperature, on the decolorization of reactive black 5 and methylene blue dyes. To study the effect of the photocatalyst loading on the decolorization of reactive black 5 and methylene blue dyes, we varied the photocatalyst amount from 0.1 to 0.5 g/l while keeping the dye concentration constant (10 ppm), and the results are shown in Figure 8A and B. The results demonstrate that the percentage decolorization of reactive black 5 and methylene blue dyes increased with the catalyst amount. The highest percentage decolorization was observed for 0.5 g/l of catalyst, suggesting that 0.5 g/l is the optimum amount; 99.02% and 73.61% of reactive black 5 and methylene blue were decolorized, respectively.

The effect of the initial dye concentration on the decolorization of dyes was determined by varying the dye concentration from 10 to 50 ppm while keeping the catalyst amount (0.5 g/l) constant, and the results are shown in Figure 9A and B. The results reveal that the percentage decolorization of dyes decreased with increasing initial dye concentration. The percentage decolorization of reactive black 5 was decreased from 99.02% to 18.93% by increasing the initial dye concentration from 10 to 50 ppm (Figure 9A). Similarly, the percentage decolorization of methylene blue was decreased from 73.61% to 1.59% (Figure 9B). This is due to the increased amount of the dye adsorption on the catalyst surface, which led to only fewer photons reaching the photocatalyst surface and a decrease in the concentration of reactive $^{\cdot}OH$ and $O_2^{\cdot-}$ radicals being produced, thereby, declining the photocatalytic decolorization efficiency.

The effect of pH on the decolorization of dyes (reactive black 5 and methylene blue) was examined by adjusting the initial pH of the dye solution from 3 to 12 while keeping the catalyst amount (0.5 g/l) and dye concentration (10 ppm) constant. The results reveal that 11 was the optimum pH for the highest percentage decolorization of dye molecules (Figure 10A and B). The photocatalyst surface charge changed with a change in pH of the initial dye solution because of the amphoteric behavior of a semiconducting photocatalyst. In acidic solutions (pH < 5), the dye photodegradation is retarded by the high concentration of protons, resulting in lower degradation efficiency. However, in alkaline solutions (pH > 10), the presence of hydroxyl ions neutralizes the acidic end products of the photodegradation reaction.

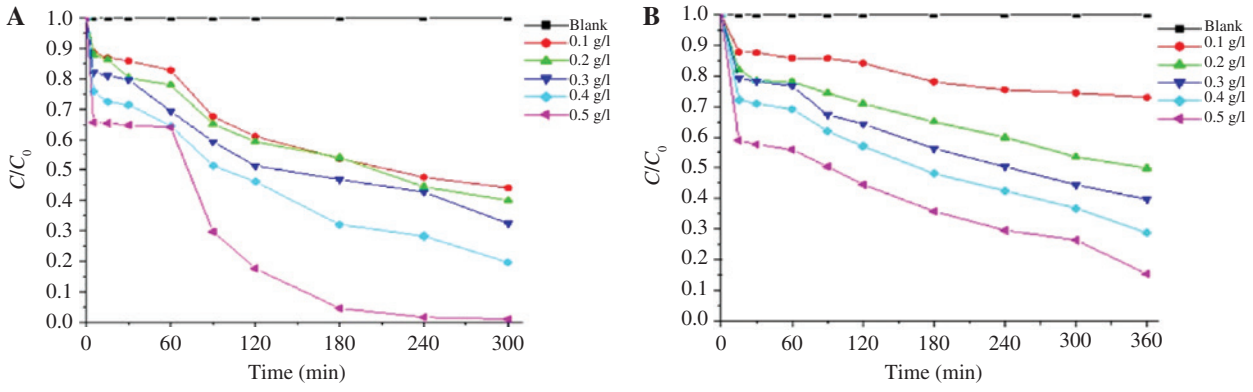

Figure 8: Effect of photocatalyst on the decolorization of (A) reactive black 5 and (B) methylene blue dyes.

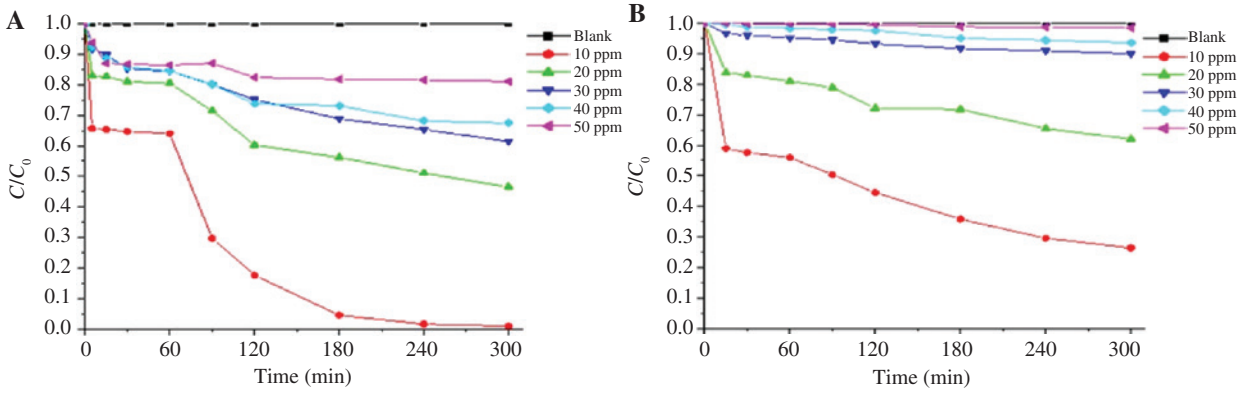

Figure 9: Effect of the initial dye concentration on the decolorization of (A) reactive black 5 and (B) methylene blue dyes.

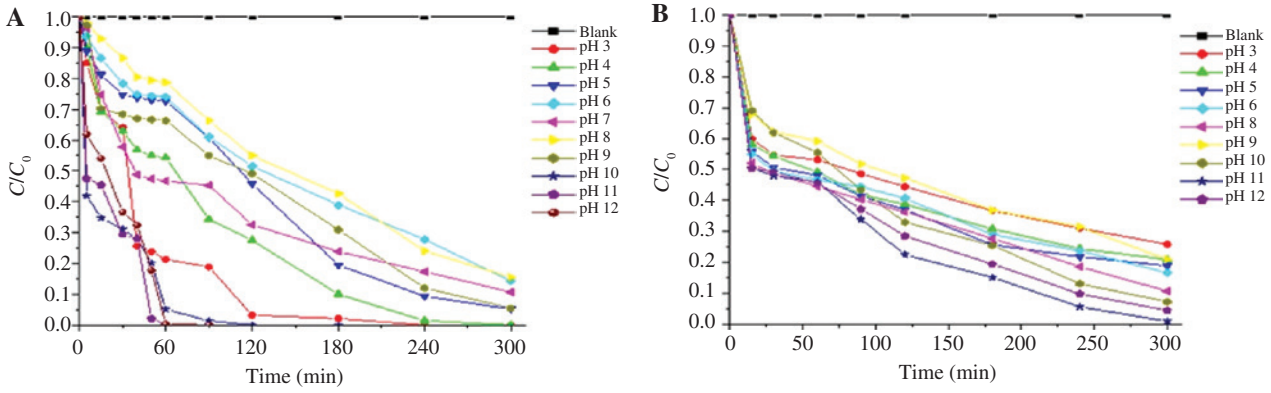

Figure 10: Effect of pH on the decolorization of (A) reactive black 5 and (B) methylene blue dyes.

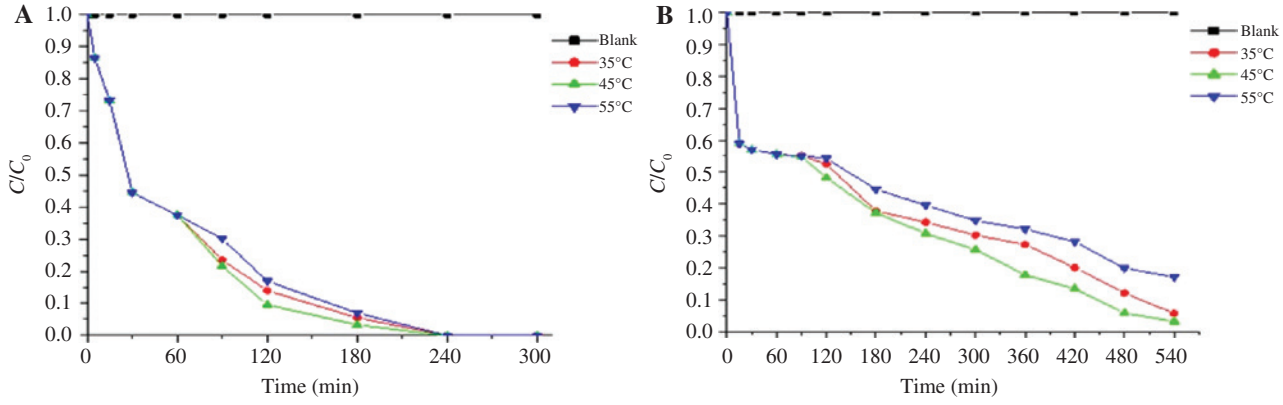

Figure 11: Effect of temperature on the decolorization of (A) reactive black 5 and (B) methylene blue dyes.

The effect of temperature on the decolorization of reactive black 5 and methylene blue dyes was investigated at 35°C, 45°C and 55°C, with the photocatalyst amount and dye concentration maintained at 0.5 g/l and 10 ppm, respectively. The results are shown in Figure 11A and B. The results reveal that a higher percentage decolorization of reactive black 5 and methylene blue dyes was observed at 45°C. This may be due to the increased adsorption of pollutants on the catalytic surface at a higher reaction temperature, which led to a higher percentage decolorization of dyes. Furthermore, the increase in temperature improved the decolorization reaction and overcame the electron-hole (e^-–h^+) recombination. However, further increasing the temperature to 55°C resulted in an increase

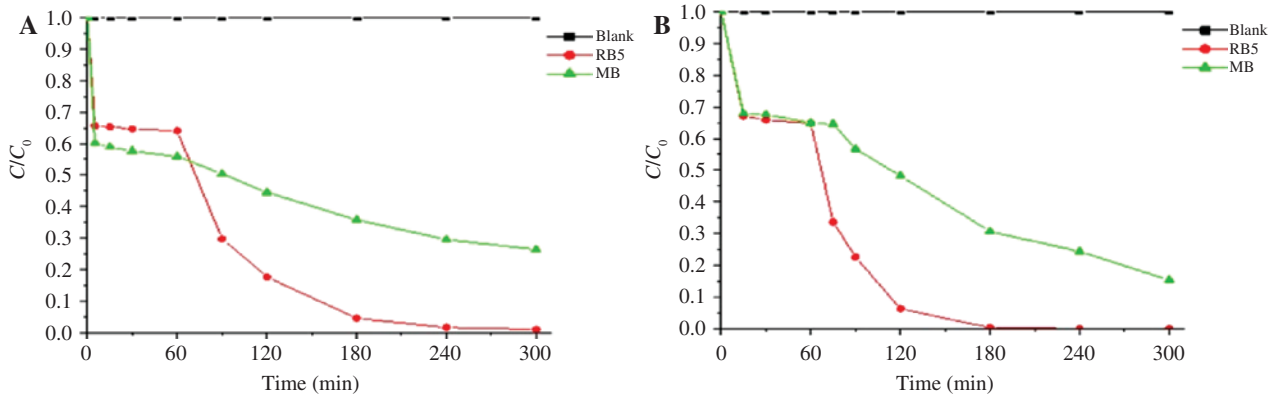

Figure 12: Photocatalytic decolorization of reactive black 5 and methylene blue dyes under (A) visible light (B) direct sunlight irradiation.

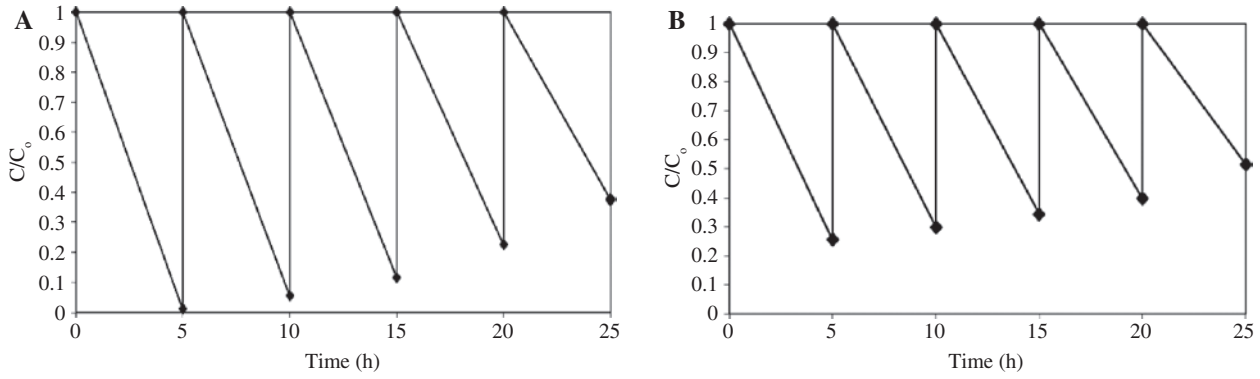

Figure 13: Recyclability of a ternary composite photocatalyst for the decolorization of (A) reactive black 5 and (B) methylene blue dyes under visible light irradiation.

in the adsorption quantity of pollutants, which decreased the light intensity reaching the catalyst surface and the subsequent production of reactive radicals. In addition, lowering the temperature favored the adsorption of the final reaction product, whose desorption tended to inhibit the reaction. At a low reaction temperature, the desorption of the formed products limited the reaction because it was slower than the degradation on the catalyst surface and the adsorption of the pollutants [41].

From the results, we observed that 30% g-C_3N_4/Bi_2MoO_6/5%TiO_2 nanotube was the best visible light active photocatalyst for the decolorization of reactive black 5 and methylene blue dyes. Therefore, to validate its visible light activity, we investigated the photocatalytic decolorization efficiency of the ternary composite under sustainable direct sunlight irradiation, and the results are shown in Figure 12A and B. The results reveal that the photocatalytic decolorization efficiency under direct sunlight was faster than under artificial visible light irradiation.

3.5 Stability and recyclability of photocatalysts

The photocatalyst stability was evaluated through a recycling test on the decolorization of reactive black 5 and methylene blue dyes using a ternary composite photocatalyst (g-C_3N_4/Bi_2MoO_6/TiO_2 nanotube) under visible light irradiation. Each cycle was for 5 h, which consisted of 1-h adsorption followed by 4-h reaction under light irradiation, and the results are shown in Figure 13A and B. The results demonstrate that the photocatalytic decolorization efficiency of the ternary composite was not reduced after five cycles of decolorization experiments; however, the percentage decolorization of reactive black 5 and methylene blue dyes was decreased to 70% and 50%, respectively. This may be due to the adsorption of dye molecules on the surface of the ternary composite photocatalyst (g-C_3N_4/Bi_2MoO_6/TiO_2 nanotube), which decreases the light intensity that reaches the photocatalyst surface and

declines the percentage decolorization of dyes. From the recyclability test, it was further confirmed that the ternary composite photocatalyst (g-C_3N_4/Bi_2MoO_6/TiO_2 nanotube) was highly stable and reusable, and it could be promoted for practical applications.

3.6 Kinetic study

The enhanced photocatalytic decolorization efficiency of the ternary composite photocatalyst (g-C_3N_4/Bi_2MoO_6/TiO_2 nanotube) was confirmed by a kinetic study. It was observed that the photocatalytic decolorization of dyes followed pseudo first-order kinetics in association with the Langmuir-Hinshelwood mechanism, as shown in Eq. (1) (C_0 is the initial dye concentration, C_t is the concentration at a given time (t), and k is the first order rate constant) [42].

$$-\ln(C_o/C_t) = k \times t \quad (1)$$

The kinetic study on the decolorization of reactive black 5 dye was conducted. The rate constant was calculated from the slope of $\ln(C_o/C_t)$ vs. time plot, and the results are tabulated in Table 1. The results demonstrate that the ternary composite photocatalyst (g-C_3N_4/Bi_2MoO_6/TiO_2 nanotube) shows a higher rate constant (0.0159 min^{-1}) compared with the TiO_2 nanotube (0.0122 min^{-1}), g-C_3N_4 (0.0084 min^{-1}), Bi_2MoO_6 (0.0012 min^{-1}), g-C_3N_4/Bi_2MoO_6 (0.0101 min^{-1}), and P25 TiO_2 (0.0028 min^{-1}); the correlation coefficient R^2 was 0.9719 (Table 1). From the results, we conclude that the use of a ternary composite photocatalyst (g-C_3N_4/Bi_2MoO_6/TiO_2 nanotube) yields a higher visible light photocatalytic decolorization efficiency compared with the use of the other photocatalysts listed in Table 1.

Table 1: Kinetic constants for the photocatalytic decolorization of reactive black 5 dye.

Photocatalyst	R^2	k (min^{-1})
g-C_3N_4	0.8876	0.0084
Bi_2MoO_6	0.7622	0.0012
TiO_2 P25	0.5404	0.0028
TiO_2 nanotube	0.8736	0.0122
g-C_3N_4/Bi_2MoO_6	0.9588	0.0101
g-C_3N_4/Bi_2MoO_6/TiO_2 nanotube	0.9719	0.0159

3.7 Mechanism of photocatalytic decolorization

Under visible light irradiation, Bi_2MoO_6, g-C_3N_4, and TiO_2 nanotube photocatalysts are excited; then, the excited electrons are transferred to the conduction band (CB) and leave behind a hole in the valence band (VB), generating e^-–h^+ pairs in each photocatalytic material. From the literature, it is understood that VB and CB positions of g-C_3N_4, Bi_2MoO_6, and TiO_2 are –1.13 and +1.57 eV, –0.32 and +2.44 eV, and –0.2 and +3.0 eV, respectively [29, 43]. Therefore, photogenerated e^-–h^+ pairs are efficient, transferring electrons from a higher CB of g-C_3N_4 to the CB of Bi_2MoO_6 and then to the CB of TiO_2 nanotube, which react with the adsorbed O_2 to

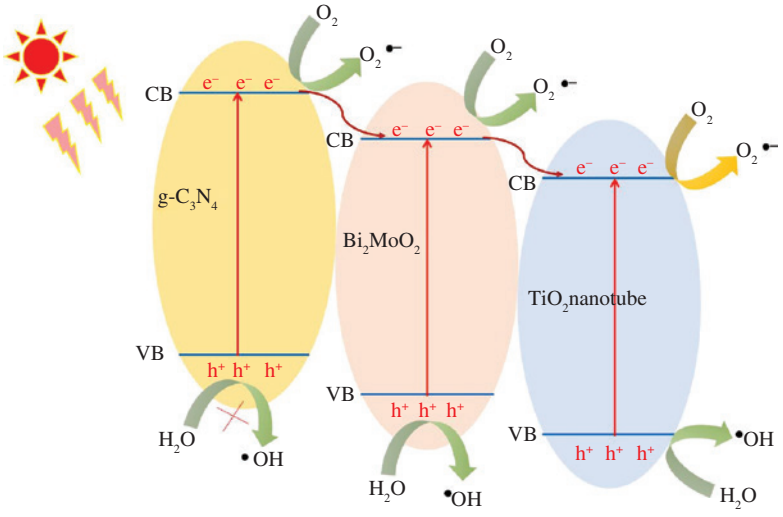

Figure 14: Probable mechanism of the separation of photogenerated e^-–h^+ pairs during the decolorization of dye caused by a ternary composite photocatalyst (g-C_3N_4/Bi_2MoO_6/TiO_2 nanotube).

yield a reactive superoxide radical ion ($O_2^{\bullet-}$) and enhance its decolorization efficiency. Similarly, the holes in VB of the TiO_2 nanotube are transferred to the VB of Bi_2MoO_6 and then to the VB of g-C_3N_4. Figure 14 depicts the probable charge separation processes in a ternary composite photocatalyst (g-C_3N_4/Bi_2MoO_6/TiO_2 nanotube) during the photocatalytic decolorization of dye molecules. However, the accumulated holes in the VB of g-C_3N_4 cannot oxidize the H_2O or surface-adsorbed –OH groups into hydroxyl radicals ($^{\bullet}OH$) because the VB potential of CN (+1.57 eV) is much lower than the required potential for $^{\bullet}OH$ generation ($H_2O/^{\bullet}OH = +2.4$ eV). However, the VB positions of Bi_2MoO_6 and TiO_2 nanotube are sufficient to oxidize the water molecules and produce reactive $^{\bullet}OH$ radicals. Therefore, as discussed above, the photogenerated e^-–h^+ pairs are separated, producing reactive radicals ($^{\bullet}OH$ and $O_2^{\bullet-}$) in the ternary composite. On the other hand, holes in the VB of Bi_2MoO_6 and the TiO_2 nanotube may directly oxidize the dye molecules and enhance the decolorization efficiency. Furthermore, the electrons in the CB of g-C_3N_4, Bi_2MoO_6 and TiO_2 nanotube may also directly react with the adsorbed O_2 and produce $O_2^{\bullet-}$. The reactive radical species are reacted with the dye molecule, producing a range of intermediates, which are further mineralized into carbon dioxide, water, and inorganic nitrogen with ammonium and nitrate ions. These photogenerated electrons and hole transfer processes can be described as follows:

$$\text{g-}C_3N_4 + h\nu\,(\text{visible light}) \rightarrow \text{g-}C_3N_4(e_{CB}^- + h_{VB}^+)$$

$$Bi_2MoO_6 + h\nu\,(\text{visible light}) \rightarrow Bi_2MoO_6(e_{CB}^- + h_{VB}^+)$$

$$TiO_2\,\text{nanotube} + h\nu\,(\text{visible light}) \rightarrow TiO_2\,\text{nanotube}\,(e_{CB}^- + h_{VB}^+)$$

$$TiO_2\ \text{nanotube}(e_{CB}^- + h_{VB}^+) + \text{g-}C_3N_4(e_{CB}^- + h_{VB}^+) + Bi_2MoO_6(e_{CB}^- + h_{VB}^+) \rightarrow TiO_2\ \text{nanotube}(e_{CB}^-) + \text{g-}C_3N_4(h_{VB}^+)$$

$$\text{g-}C_3N_4(h_{VB}^+) + H_2O \text{ or } OH \rightarrow \text{No formation of } {}^{\bullet}OH$$

$$TiO_2\ \text{nanotube}\ (e_{CB}^-) \text{ or g-}C_3N_4(e_{CB}^-) \text{ or } Bi_2MoO_6(e_{CB}^-) + O_2 \rightarrow O_2^{\bullet-} + TiO_2\ \text{nanotube or g-}C_3N_4 \text{ or } Bi_2MoO_6$$

$$Bi_2MoO_6(h_{VB}^+) + H_2O \text{ or } OH \rightarrow Bi_2MoO_6 + {}^{\bullet}OH$$

$$TiO_2\ \text{nanotube}\ (h_{VB}^+) + H_2O \text{ or } OH \rightarrow TiO_2\ \text{nanotube} + {}^{\bullet}OH$$

$$Bi_2MoO_6(h_{VB}^+) + TiO_2\ \text{nanotube}\ (h_{VB}^+) + \text{reactive black 5 dye or methylene blue dye} \rightarrow \text{oxidized products}$$

$$O_2^{\bullet-} + {}^{\bullet}OH + \text{reactive black 5 dye or methylene blue dye} \rightarrow \text{intermediate products} \rightarrow CO_2 + H_2O + NH_4^+ + NO_3^-$$

4 Conclusions

Ternary composite photocatalysts (g-C_3N_4/Bi_2MoO_6/TiO_2 nanotube) were successfully synthesized through simple solid combustion, hydrothermal and wetness impregnation methods. Powder XRD analysis confirms the phase purity and crystallinity of unitary (g-C_3N_4, Bi_2MoO_6 and TiO_2 nanotube), binary composite and ternary composite photocatalysts. The layered structure of g-C_3N_4 and the plate-like structure of Bi_2MoO_6 and the formation of binary and ternary composites are confirmed by SEM analysis. EDX analysis confirms the presence of C, N, Bi, Mo, O and Ti elements in the ternary composite, and no impurities were observed. The photocatalytic activity evaluation results reveal that the highest decolorization percentage of reactive black 5 and methylene blue dyes was obtained at an optimum catalyst amount of 0.5 g/l, an initial dye concentration of 10 ppm, a pH of 11 and a temperature of 45°C. The recyclability test demonstrates that the synthesized ternary composite photocatalyst was highly stable up to five cycles of decolorization reactions. Kinetic analysis reveals that the dye decolorization follows pseudo first-order kinetics. From the results, we conclude that ternary composite photocatalysts (g-C_3N_4/Bi_2MoO_6/TiO_2 nanotube) are efficient solar light-active photocatalysts for the decolorization of reactive black 5 and methylene blue dyes under the applied experimental conditions.

Acknowledgments: The authors are thankful to the Taiwan Ministry of Science and Technology (MOST 105-2811-E-033-001) for the financial support.

References

[1] Zangeneh H, Zinatizadeh AAL, Habibi M, Akia M, Hasnain Isa M. *J. Ind. Eng. Chem.* 2015, 26, 1–36.
[2] Fathima NN, Aravindhan R, Rao JR, Nair BU. *Chemosphere* 2008, 70, 1146–1151.
[3] Kerkez-Kuyumcu Ö, Kibar E, Dayioglu K, Gedik F, Akin AN, Ozkara Aydinoglu S. *J. Photochem. Photobiol. A* 2015, 311, 176–185.
[4] Ahmad A, Mohd-Setapar SH, Chuong CS, Khatoon A, Wani WA, Kumar R, Rafatullah M. *RSC Adv.* 2015, 5, 30801–30818.
[5] Khan E, Li M, Huang CP. *Water Environ. Res.* 79, 2007, 1858–1902.
[6] Banerjee S, Pillai SC, Falaras P, O'Shea KE, Byrne JA, Dionysiou DD. *J. Phys. Chem. Lett.* 2014, 5, 2543–2554.

[7] Pelaez M, Nolan NT, Pillai SC, Seery MK, Falaras P, Kontos AG, Dunlop PSM, Hamilton JWJ, Byrne JA, O'Shea K, Entezari MH, Dionysiou DD. *Appl. Catal. B* 2012, 125, 331–349.
[8] Hoffmann MR, Martin ST, Choi W, Bahnemann DW. *Chem. Rev.* 1995, 95, 69–96.
[9] Fujishima A, Honda K. *Nature* 1972, 238, 37–38.
[10] Fujishima A, Rao TN, Tryk DA. *J. Photochem. Photobiol. C* 2000, 1, 1–21.
[11] Linsebigler AL, Lu G, Yates JT. *Chem. Rev.* 1995, 95, 735–758.
[12] Rawal SB, Bera S, Lee D, Jang DJ, Lee WI. *Catal. Sci. Technol.* 2013, 3, 1822–1830.
[13] Kasuga T, Hiramatsu M, Hoson A, Sekino T, Niihara K. *Langmuir* 1998, 14, 3160–3163.
[14] Kasuga T, Hiramatsu M, Hoson A, Sekino T, Niihara K. *Adv. Mater.* 1999, 11, 1307–1311.
[15] Xu JC, Lu M, Guo XY, Li HL. *J. Mol. Catal. A.* 2005, 226, 123–127.
[16] Zhang SM, Chen YY, Yu Y, Wu HH, Wang SR, Zhu BL, Huang WP, Wu SH. *J. Nanopart. Res.* 2008, 10, 871–875.
[17] Natarajan TS, Natarajan K, Bajaj HC, Tayade RJ. *J. Nanopart. Res.* 2013, 15, 1–18.
[18] Wang XC, Maeda K, Thomas A, Takanabe K, Xin G, Carlsson JM, Domen K, Antonietti M. *Nat. Mater.* 2009, 8, 76–80.
[19] Yan SC, Li ZS, Zou ZG. *Langmuir* 2009, 25, 10397–10401.
[20] Cao S, Low J, Yu J, Jaroniec M. *Adv. Mater.* 2015, 27, 2150–2176.
[21] Zhao H, Tian F, Wang R, Chen R. *Rev. Adv. Sci. Eng.* 2014, 3, 3–27.
[22] Li ZQ, Chen XT, Xue ZL. *Cryst. Eng. Comm.* 2013, 15, 498–508.
[23] Zhang M, Shao C, Mu J, Huang X, Zhang Z, Guo Z, Zhang P, Liu Y. *J. Mater. Chem.* 2012, 22, 577–584.
[24] Bi J, Che J, Wu L, Liu M. *Mater. Res. Bull.* 2013, 48, 2071–2075.
[25] Dong G, Zhang Y, Pan Q, Qiu J. *J. Photochem. Photobiol. C* 2014, 20, 33–50.
[26] Li H, Liu J, Hou W, Du N, Zhang R, Tao X. *Appl. Catal. B* 2014, 160, 89–97.
[27] Sridharan K, Jang E, Park TJ. *Appl. Catal. B* 2013, 142, 718–728.
[28] Shen J, Yang H, Shen Q, Feng Y, Cai Q. *Cryst. Eng. Comm*. 2014, 16, 1868–1872.
[29] Jo WK, Natarajan TS. *Chem. Eng. J.* 2015, 281, 549–565.
[30] Li N, Zhu L, Zhang WD, Yu YX, Zhang WH, Hou MF. *J. Alloys Comp.* 2011, 509, 9770–9775.
[31] Zhang M, Shao C, Mu J, Zhang Z, Guo Z, Zhang P, Liu Y. *Cryst. Eng. Comm*. 2012, 14, 605–612.
[32] Fu D, Han G, Liu F, Xiao Y, Wang H, Liu R, Liu C. *Mater. Sci. Semicond. Process.* 2014, 27, 966–974.
[33] Li J, Liu Y, Li H, Chen C. *J. Photochem. Photobiol. A* 2016, 317, 151–160.
[34] Li J, Liu X, Sun Z, Pan L. *J. Colloid Interface Sci.* 2016, 463, 145–153.
[35] Li H, Zhang T, Pan C, Pu C, Hu Y, Hu X, Liu E, Fan J. *Appl. Surf. Sci.* 2017, 391, 303–310.
[36] Wen J, Xie J, Chen X, Li X. *Appl. Surf. Sci.* 2017, 391, 72–123.
[37] Min Z, Wang Z, Li Y, Jiang J, Li J, Qian D, Li J. *Mater. Lett.* 2017, 193, 18–21.
[38] Chen W, Duan GR, Liu TY, Chen SM, Liu XH. *Mater. Sci. Semicond. Process.* 2015, 35, 45–54.
[39] Jiang D, Zhu J, Chen M, Xie J. *J. Colloid Interface Sci.* 2014, 417, 115–120.
[40] Natarajan TS, Bajaj HC, Tayade RJ. *J. Colloid Interface Sci.* 2014, 433, 104–114.
[41] Soares ET, Lansarin MA, Moro CC. *Braz. J. Chem. Eng.* 2007, 24, 29–36.
[42] Hou L, Hua H, Gan L, Yuan C. *Mater. Lett.* 2015, 159, 35–38.
[43] Xu YS, Zhang WD. *Dalton Trans.* 2013, 42, 1094–1101.